Research Paper

# m6A-dependent upregulation of TRAF6 by METTL3 is associated with metastatic osteosarcoma

Jing Wang [a,1], Wentao Wang [b,1], Xing Huang [a,1], Jiashi Cao [a], Shuming Hou [a], Xiangzhi Ni [a], Cheng Peng [a], Tielong Liu [a,*]

[a] Department of Orthopaedic Oncology, Spinal Tumor Center, Shanghai Changzheng Hospital, Naval Medical University, Shanghai 200003, PR China
[b] Department of Orthopedics, Shanghai Changhai Hospital, Naval Medical University, Shanghai 200433, PR China

## ARTICLE INFO

## ABSTRACT

*Objectives:* RNA N6-methyladenosine (m6A) is associated with tumorigenesis. The importance of methyltransferase-like 3 (METTL3) has been reported in cancer progression and metastasis. However, its role and molecular mechanism in osteosarcoma (OS), the most common primary bone tumor, is poorly studied. In this study, we aimed to investigate the functional role and underlying mechanism of METTL3 in the metastasis of OS.
*Methods:* The expression differences of METTL3 between metastatic and non-metastatic OS tissues and patients with different Enneking stages were detected using RT-qPCR. METTL3 was artificially downregulated in the cells, followed by wound healing assay, Matrigel assay, immunofluorescence, *in vivo* tumorigenic assay, HE staining, and western blot. Transcriptome sequencing and m6A-seq was conducted to identify the downstream genes of METTL3, and RIP and dual-luciferase assays were performed for validation. The expression of TRAF6 in OS tissues was detected using RT-qPCR. Finally, the rescue experiments were conducted.
*Results:* METTL3 was overexpressed in metastatic OS tissues, and downregulation of METTL3 decreased cell migration, invasion, epithelial-mesenchymal transition, and tumorigenic and metastatic activities. The m6A site was highly enriched in cells poorly expressing METTL3, and the m6A peak was mainly enriched in the exon region. METTL3 was positively correlated with TRAF6 in metastatic OS, and depletion of METTL3 resulted in the loss of TRAF6 expression in OS cells. Upregulation of TRAF6 contributed to metastases *in vitro* and *in vivo*.
*Conclusion:* METTL3 is highly expressed in OS and enhances TRAF6 expression through m6A modification, thereby promoting the metastases of OS cells.

## 1. Introduction

Osteosarcoma (OS) is a high-grade primary skeletal tumor characterized by spindle cells of mesenchymal source depositing immature osteoid matrix [1]. A notable characteristic of this malignancy is the high tendency to metastasize into the lungs, and about 20% of patients show radiologically detectable lung metastases at diagnosis and almost all of them have microscopic lesions which become evident during the course of the disease [2]. The presence of metastatic disease is a strong indicator of poor prognosis of OS, and the prognosis of metastatic patients depends approximately utterly on the metastasis and drug resistance, particularly the status of lung metastasis [3]. Therefore, clarifying the molecular mechanisms underlying metastasis in OS is of great importance for the improvement of patents' prognoses.

RNA methylation has been acknowledged as a vital regulator of transcript expression, and the most common RNA methylation, N6-methyladenosine (m6A), occurs in about a quarter of transcripts at the genome-wide level and is enriched around stop codons, in 5'- and 3'-untranslated regions (5'UTR and 3'UTR), and within long internal exons [4]. The m6A editing has been implicated in mRNA degradation, protein translation as well as RNA splicing, and they have been associated with obesity, cancers, and other human diseases [5]. The deposition of m6A is catalyzed by the m6A methyltransferase complex which is comprised of methyltransferase-like 3 (METTL3) and METTL14) (i.e., writers) and their cofactor, Wilms

* Corresponding author at: Department of Orthopaedic Oncology, Spinal Tumor Center, Shanghai Changzheng Hospital, Naval Medical University, No. 415, Fengyang Road, Huangpu District, Shanghai 200003, PR China.
  *E-mail address:* Dr_Tielong1271@126.com (T. Liu).
  [1] These authors contributed equally to this work.

tumor 1-associated protein (WTAP) [6]. m6A is involved in the progression of various cancers, including glioma, breast cancer, and hepatoblastoma [7–9]. The inhibition of METTL3 has recently been proposed as a potential therapeutic strategy against myeloid leukemia, and provide proof of concept that the targeting of RNA-modifying enzymes represents a promising avenue for anticancer therapy [10]. Additionally, knockout of METTL3 remarkably suppressed tumorigenicity and lung metastasis in hepatocellular carcinoma [11]. More relevantly, high expression of METTL3 was associated with poor prognosis in OS [12]. Therefore, we set to define the effects and the mechanism of action underlying METTL3 on metastasis in OS. As for the downstream effector, tumor necrosis factor receptor-associated factor 6 (TRAF6) has been revealed as an oncogene in OS by enhancing cell proliferation, apoptosis and invasion [13]. The suppression of TRAF6 by silencing RNA decreased multiple myeloma cell proliferation and increased apoptosis [14]. But its specific upstream mechanism in OS remains largely unclear. Given the significant role of METTL3 and TRAF6 in cancer and the potential of these molecules as new therapeutic targets for OS, herein we aim to expound the possible correlation of METTL3 and TRAF6 in OS and elucidate the precise molecular mechanism.

## 2. Materials and methods

### 2.1. Patients and clinical samples

The human samples were obtained according to the principles of the *Declaration of Helsinki* and approved by Shanghai Changzheng Hospital. Written informed consent was acquired from all patients and/or their legal guardians. Fifty-eight patients with OS treated at Shanghai Changzheng Hospital between January 2013 and January 2016 were selected for this study, and none of the admitted patients received preoperative anti-tumor therapy including radiotherapy and chemotherapy. Tissue samples were placed in liquid nitrogen and stored in a −80 °C refrigerator for subsequent studies. Fifty-eight patients with OS were effectively followed-up for five years, at an interval of three months.

### 2.2. RT-qPCR

Total RNA was isolated using TRIzol reagent (Thermo Fisher Scientific Inc., Waltham, MA, USA), and then 500 ng total RNA was reversely transcribed into cDNA using a high-volume cDNA reverse transcription kit (Thermo Fisher Scientific). RT-qPCR analysis was performed using SYBR Green PCR Master (Roche Diagnostics, Co., Ltd., Rotkreuz, Switzerland) in a 7500 fast real-time instrument (Applied Biosystems, Inc., Foster City, CA, USA) using 1 μL cDNA. GAPDH was used as a housekeeping gene to calculate the relative expression. The primers used in this study was shown in Table 1. Relative gene expression was analyzed by the $2^{-\Delta\Delta Ct}$ method.

### 2.3. Immunohistochemistry

The OS tissues were routinely paraffin-embedded and cut into 5-μm-thick sections, and then re-dewaxed and treated with hydrogen peroxide to quench the endogenous peroxidase activity. The sections were incubated with primary antibodies to METTL3 (1:500, ab195352, Abcam, Cambridge, UK) and TRAF6 (1:300, ab33915, Abcam) at 4 °C overnight. Next, the sections were re-probed with horseradish peroxidase (HRP)-coupled anti-mouse IgG (1:5000, ab205718, Abcam) at room temperature for 120 min. Immunoreactive cells were detected by Signal Stain diaminobenzidine (Cell Signaling Technologies, Beverly, MA, USA). After counter-staining with hematoxylin QS (Vector Labora-

**Table 1**
The sequence of primers.

| Gene name | Primers |
|---|---|
| METTL3 | Forward: 5′-CTGGGCACTTGGATTTAAGGAA-3′ |
| | Reverse: 5′-TGAGAGGTGGTGTAGCAACTT -3′ |
| METTL14 | Forward: 5′-GTTGGAACATGGATAGCCGC-3′ |
| | Reverse: 5′-CAATGCTGTCGGCACTTTCA-3′ |
| WTAP | Forward: 5′-GTAGACCCAGCGATCAACTTGT-3′ |
| | Reverse: 5′-GCGTAAACTTCCAGGCACTC-3′ |
| ALKBH5 | Forward: 5′-GTCCCGGGACAACTACAAGG-3′ |
| | Reverse: 5′-GATGTGGATGGGGTCAACGT-3′ |
| FTO | Forward: 5′-ACCTCCAGCATTAGATTC-3′ |
| | Reverse: 5′-GAAACTACCGCATTTACC-3′ |
| TRAF6 | Forward: 5′-TCATAATGTTAACCTCTCTT-3′ |
| | Reverse: 5′-TGTCTTACTAGGCGCCCCTC-3′ |
| GAPDH | Forward: 5′-GGTGGTCTCCTCTGACTTCAA-3′ |
| | Reverse: 5′-GTTGCTGTAGCCAAATTCGTTGT-3′ |

**Note:** METTL, methyltransferase-like; WTAP, Wilms' tumor 1-associating protein; ALKBH5, AlkB homolog 5 RNA demethylase; FTO, fat mass and obesity-associated protein; TRAF6, tumor necrosis factor receptor-associated factor 6; GAPDH, glyceraldehyde-3-phosphate dehydrogenase.

tories, Inc., Burlingame, CA, USA), random photographs were taken using an inverted microscope (Nikon Instruments Inc., Melville, NY, USA). Two experienced pathologists who were unaware of the clinicopathological data evaluated the immunostaining samples, separately.

### 2.4. LC-MS/MS analysis

Total RNA from cell and tissue samples was extracted using TRIzol (Thermo Fisher scientific), from which mRNA was purified using the NEBNext Poly(A) mRNA magnetic separation module. In a 25 μL reaction system containing 10 mM $NH_4OAc$ (pH = 5.3), approximately 200 ng purified mRNA was incubated with nuclease P1 (0.5 U, Sigma-Aldrich Chemical Company, St Louis, MO, USA) for 1 h at 42 °C, followed by the incubation with 3 μL $NH_4HCO_3$ and 1 μL alkaline phosphatase for 2 h at 37 °C. The samples were neutralized with 1 μL HCl, then diluted to 50 μL and filtered through a 0.22 μm filter (Millipore Corp, Billerica, MA, USA). All samples were separated by a C18 column using a reversed-phase ultra-high-performance-performance LC (Agilent Technologies, Santa Clara, CA, USA) and analyzed by an Agilent 6410 QQQ triple-quadrupole LC mass spectrometer using positive ion electrospray ionization mode. All nucleosides were quantified by the transition from 268.0 to 136.0 (A) and 282.1 to 150.0 (m6A). Quantification was calculated using standard curves of standards run in the same batch, and m6A/A levels were calculated from calibration curves.

### 2.5. Cell culture and treatment

OS cells U2OS, MG-63, Saos2, HOS were from the Cell Bank of Shanghai Institute of Cells (Shanghai, China). Normal human osteoblasts (NHOst) was purchased from Procell (Wuhan, Hubei, China). The cells were cultured in DMEM plus 10% FBS (Gibco, Carlsbad, CA, USA) and incubated at 37 °C and 5% $CO_2$. In order to artificially downregulate METTL3 and upregulate TRAF6, the cells were transfected with plasmids using lipofectamine 2000 (Thermo Fisher Scientific) as per the manufacturer's instructions. The plasmids were pcDNA 3.0 (Thermo Fisher Scientific), and the shRNA targeting METTL3 and the TRAF6 overexpression fragment were synthesized by Shanghai GenePharma Co., Ltd. (Shanghai, China). The cells transfected for 2 weeks were treated with G418 (700 μg/mL), and the surviving cells were selected and seeded into 96-well plates for further expansion of the monoclonal cell population. The cells were treated with 3-deazaadenosine (DAA, Sigma-Aldrich) to inhibit methylation. In brief, 200 μL DAA was mixed

with culture medium, and the cells were cultured with such culture medium in a cell incubator for 24 h. After that, the culture medium was renewed.

### 2.6. Wound healing assay

For the wound healing assay, OS cells were plated into 6-well culture plates at $2.5 \times 10^5$ cells/mL and cultured until a 90% confluence was formed. The cells were scraped with a 200 μL pipette tip to form wounds, and images were captured by a standard light microscopy (ECLIPSE TS100, Nikon) 24 h after injury. The wound healing distance was measured using ImageJ software (National Institutes of Health, Bethesda, MD, USA), and the healing rate was calculated = healing distance/wound distance ×100%.

### 2.7. Matrigel assay

For the invasion assay, polycarbonate filters (8-μm pore size, Corning Glass Works, Corning, N.Y., USA) coated with 50% Matrigel (BD bioscience, Bedford, MA, USA) were used to separate the apical and basolateral chambers. The cells after transfection were grown in 200 μL DMEM (Thermo Fisher Scientific) to prepare a cell suspension. Cell suspension ($1 \times 10^5$ OS cells) was added to the apical chamber, and 600 μL DMEM plus 10% FBS was supplemented to the basolateral chamber. After 24 h incubation, the cells in the basolateral chamber were fixed in methanol for 10 min and stained with 0.5% crystal violet. Then, photographs were randomly taken under an inverted microscope (Nikon).

### 2.8. Immunofluorescence staining

OS cells cultured in 24-well plates were fixed in 4% paraformaldehyde and permeabilized in 1% Triton X-100-phosphate buffered saline (PBS). After being blocked with 1%

BSA, the cells were incubated with primary antibodies to E-cadherin (1:500, ab11512, Abcam), METTL3 (1:300, ab216936, Abcam), Vimentin (1:300, ab193555, Abcam), and TRAF6 (1:1500, ab33915, Abcam) overnight at 4 °C and with Alexa Fluor 488-coupled secondary antibody (1:500, ab150077, Abcam) for 0.5 h at ambient temperature. Finally, the nuclei were counter-stained with 4′,6-diamidino-2-phenylindole (Beyotime, Shanghai, China), and images were obtained using a Zeiss Axio microscope (Zeiss, Oberkochen, Germany).

### 2.9. RNA immunoprecipitation (RIP)

OS cells were lysed in lysis buffer containing 150 mM KCl, 10 mM N-2-hydroxyethylpiperazine-N'-2-ethanesulfonic acid (pH = 7.6), 2 mM ethylenediaminetetraacetic acid (EDTA), 0.5% NP-40, 0.5 mM dithiothreitol (DTT), protease inhibitor mixture (1:100) and 400 U/mL RNase inhibitor. The cell lysates were centrifuged, and a 50-μL aliquot of the cell lysate was used as input and the remaining sample was incubated with 20 μL A/G magnetic beads (ProteinTech Group, Chicago, IL, USA) pre-conjugated with antibodies to IgG (1:1000, ab172730, Abcam) or TRAF6 (1:500, ab33915, Abcam) at 4 °C for 4 h. The beads were washed twice with washing buffer (50 mM Tris, 200 mM NaCl, 2 mM EDTA, 0.05% NP-40, 0.5 mM DTT and RNase inhibitor). RNA was eluted from the beads with 50 μL RLT buffer and purified with a Qiagen RNeasy column. RNA was eluted in 100 μL RNase-free water and reverse transcribed to cDNA using the PrimeScript qRT-PCR kit (Takara Biotechnology Ltd., Dalian, Liaoning, China). Enrichment foldchange was determined using RT-qPCR.

### 2.10. Animal models

The Animal Care and Use Committee of Shanghai Changzheng Hospital approved the animal handling and experimental
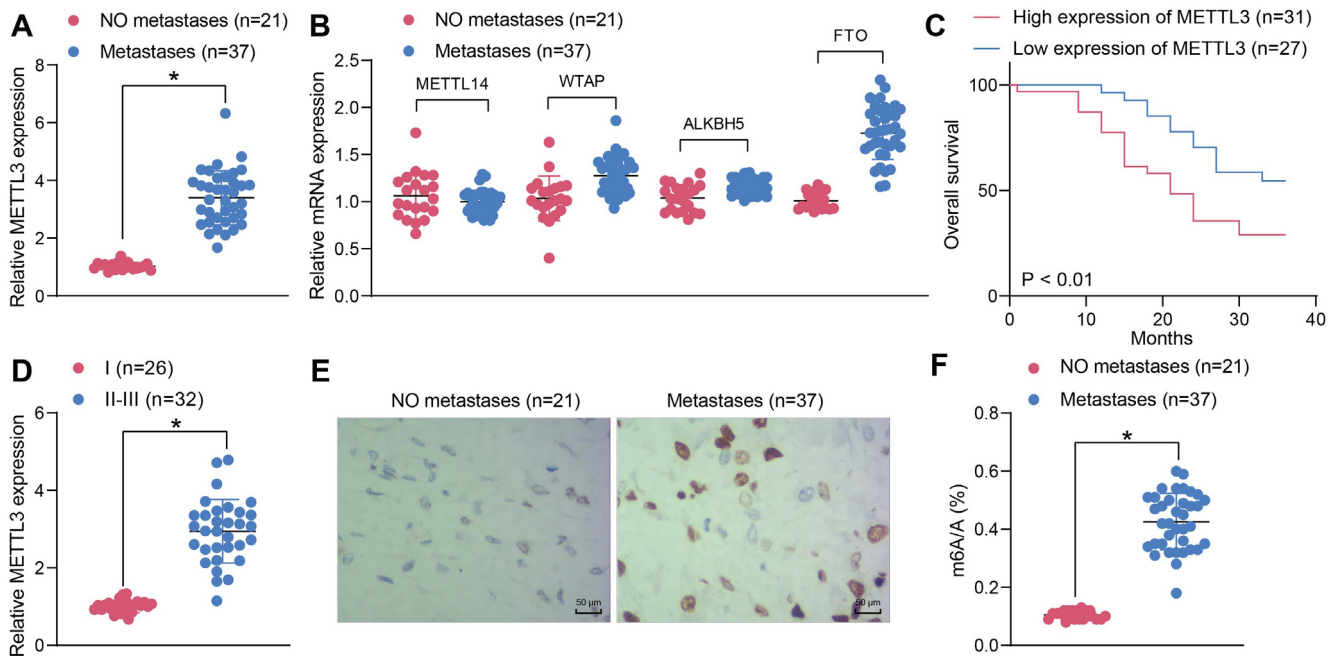


**Fig. 1.** METTL3 is elevated in OS and correlates with dismal prognosis. (A) METTL3 expression in tissues of metastatic and non-metastatic OS patients by RT-qPCR. (B) the expression of other methyltransferases in OS tissues by RT-qPCR. (C) survival analysis of patients differentially expressing METTL3 analyzed using Kaplan-Meier. (D) METTL3 expression differences between patients at different Enneking stages. (E) immunohistochemical detection of METTL3 between OS tissues from metastatic/non-metastatic patients. (F) m6A mRNA expression differences in OS tissues by m6A analysis. All the experiments were repeated at least three times, and data are represented as mean ± SD. These data were analyzed by unpaired $t$ test. *$p < 0.05$.

procedures. For mouse xenograft tumor model, $1 \times 10^6$ Saos2 or HOS cells were mixed in 200 μL PBS and injected subcutaneously into 6- to 8-week-old C57BL/6 mice (n = 5 per group, weight 20 ± 2 g, Beijing Vital River Laboratory Animal Technology Co., Ltd., Beijing, China). Tumor size of mice was measured by vernier calipers every week after injection. The mice were euthanized after 28 days by intraperitoneal injection of 1% pentobarbital sodium (120 mg/kg), and the tumor tissues were removed from the mice. The tumor volume was determined using the following formula: V (mm$^3$) = a × b$^2$/2, where "a" and "b" denote the long and short diameters, respectively.

For the lung metastasis model, $2.5 \times 10^6$ stably transfected Saos2 or HOS cells in 200 μL PBS were injected into C57BL/6 mice (n = 5) via the tail vein. After 45 days, the mice were subjected to an intraperitoneal injection of fluorescein at 300 mg/kg. After 10 min, the intensity of lung light radiation in mice with lung metastases was determined using the IVIS-100 system (Caliper Life Sciences, MA, USA). All mice were euthanized by intraperitoneal injection of 1% pentobarbital sodium (120 mg/kg). Hematoxylin-eosin (HE) staining kits (Beijing Solarbio Science & Technology Co., Ltd., Beijing, China) were utilized to observe the formation of lung metastases. The tissues were dewaxed with xylene for 8 min, soaked in gradient concentration alcohol, stained with hematoxylin for 15 min. After removing excess staining solution with 1% hydrochloric acid alcohol for 30 s, the sections were stained with eosin solution for 5 min, dehydrated in gradient concentration alcohol, cleared in xylene for 10 min, and sealed with gum. The lung tissue sections were observed under a microscope (Nikon), and five fields of view were randomly selected for photography.

### 2.11. Western blot

For protein blot analysis, cells and tissues were harvested and lysed with radio immunoprecipitation assay buffer (Sigma-Aldrich). Protein concentrations were assessed using a BCA kit (Beyotime). Samples were separated by 10% sodium dodecyl sulphate polyacrylamide gel electrophoresis, and blots were transferred to nitrocellulose membranes (Millipore). The membranes were incubated overnight at 4 °C with primary antibodies to E-cadherin (1:2000, 13-1700, Thermo Fisher Scientific), METTL3 (1:1500, ab195352, Abcam), Vimentin (1:1000, MA5-14564,
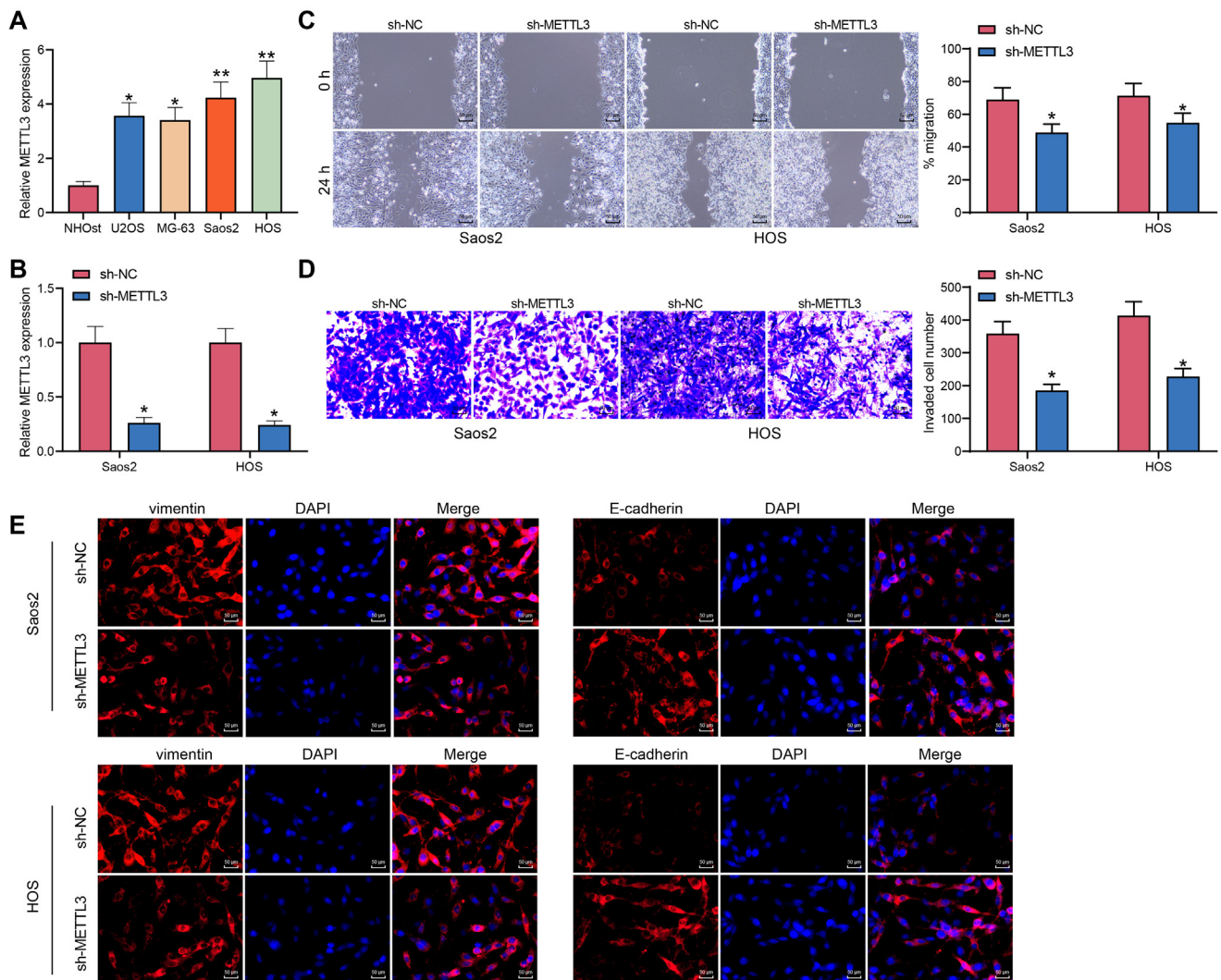


**Fig. 2.** METTL3 silencing inhibits cell invasion, migration, and EMT in OS cell lines. (A) METTL3 mRNA expression in OS cells and NHOst cells by RT-qPCR. (B) the transfection efficiency of sh-METTL3 determined using RT-qPCR. (C) migration of OS cells determined using wound healing assay. (D) invasion of OS cells determined using Matrigel invasion assay. (E) EMT process of OS cells determined using immunofluorescence staining. All the experiments were repeated at least three times, and data are represented as mean ± SD. These data were analyzed by one-way/two-way ANOVA followed by Tukey's post-tests. *$p < 0.05$, **$p < 0.01$.

Thermo Fisher Scientific), TRAF6 (1:1500, ab33915, Abcam), and GAPDH (1:1800, NB300-322, Novus Biological Inc., Littleton, CO, USA). The membranes were rinsed with Tris-buffered saline with Tween three times, followed by incubation with HRP-conjugated secondary mouse antibody to IgG (1:5000, ab205718, Abcam) for 7 h at room temperature. The membranes were developed using electrochemiluminescence (Sigma-Aldrich) and visualized using Tanon 5500.

## 2.12. Transcriptome sequencing and m(6)A-specific MeRIP-Seq

Total RNA was isolated from HOS cells using the TRIzol reagent (Thermo Fisher Scientific) and FastTrack MAGMaxi mRNA isolation kit (Thermo Fisher Scientific). RNA fragmentation, m6A-seq and library preparation were commissioned to CloudSeq Biotech (Shanghai, China). Library preparation was performed using the NEBNext Super Directional RNA Library Preparation Kit (New England BioLabs, Ipswich, MA, USA). Significant peaks with false discovery rate (FDR) <0.01 were obtained and annotated into the RefSeq database, and sequences were identified using Homer (Hypergeometric Optimization of Motif EnRichment). Cuffdiff (Cufflinks, USA) was used to find the corresponding modified genes.

HOS cells with low expression of METTL3 and control cells were pre-hybridized with DNA. Whole transcriptome libraries were prepared using the Ribo-Zero Magnetic Gold kit (Illumina, San Diego, CA, USA) and the NEBNext RNA Library Preparation Kit (New England Biolabs). Quality control and quantification were performed by BioAnalyzer 2100 system (Kapa Biosystems, USA), and the resulting libraries were sequenced and analyzed for differentially expressed mRNAs on a HiSeq2000 instrument (Illumina).

## 2.13. Dual-luciferase reporter assay

The luciferase assay was performed using lysis solution (Promega Corporation, Madison, WI, USA) and luciferase assay reagent according to the manufacturer's instructions. pmiRGLO-wild type (WT) or pmiRGLO-mutant (MT) with sh-METTL3 were co-transfected into Saos2 and HOS cells in 12-well plates, respectively. After 6 h of transfection, each cell line was re-seeded into 96-well plates, and luciferase activity was measured using Exfect transfection reagent (NanJing Vazyme Biotech Co., Ltd, Nanjing, Jiangsu, China) using a dual-luciferase assay system (Promega). The ratio of firefly to Renilla luciferase intensity was measured as an index of luciferase activity.

## 2.14. Statistical analyses

All statistical analyses were performed with SPSS 22.0 software (IBM Corp. Armonk, N.Y., USA). Data were presented as the mean ± standard deviation (SD). The differences among/between sample groups were analyzed by one-way/two-way ANOVA, followed by Tukey's post-tests, or unpaired $t$ test. Statistical significance was assigned at $p < 0.05$. All the experiments of cell lines were performed three times with triplicate samples.

## 3. Results

### 3.1. METTL3 is overexpressed in OS and has prognostic values

To explore the expression of major m6A methyltransferases in OS, we first collected OS tissues from biopsies of OS patients
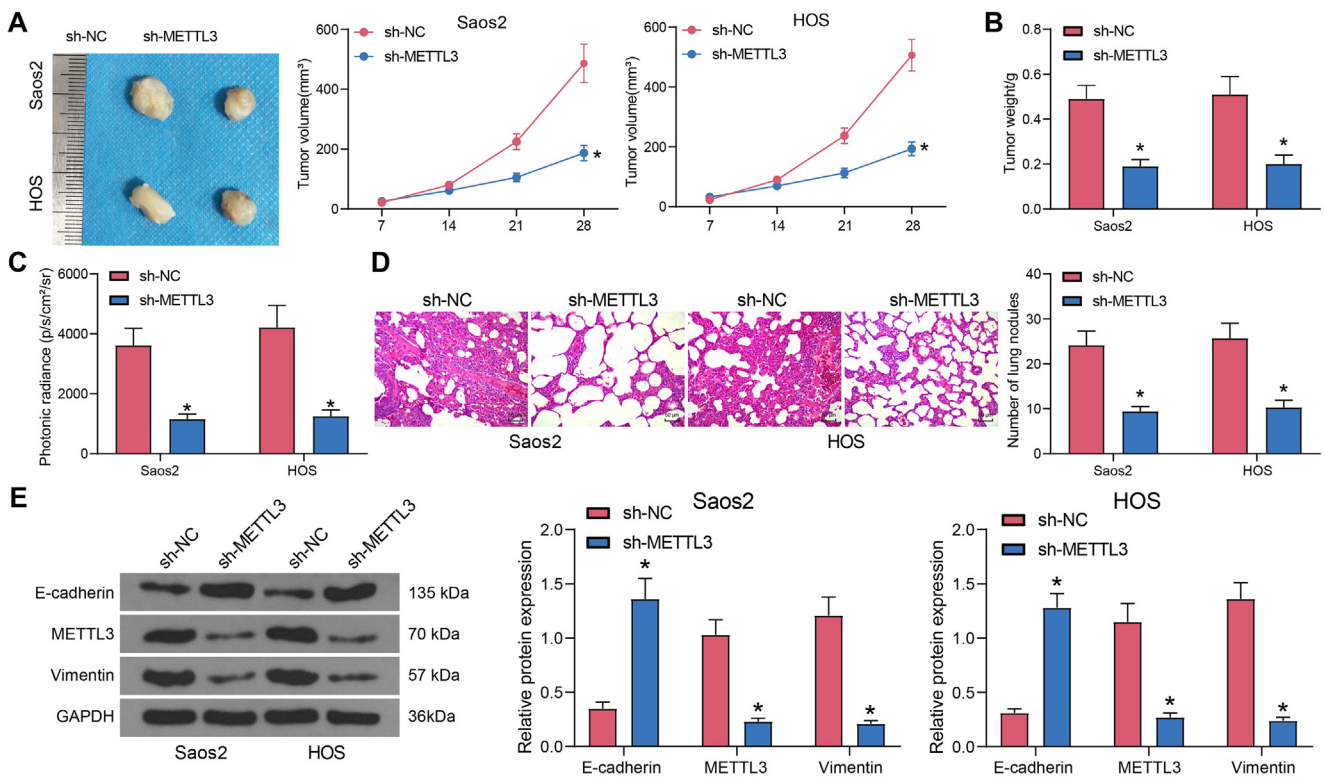


**Fig. 3.** METTL3 silencing inhibits OS cell tumorigenic and metastatic properties *in vivo*. (A) representative tumor images and tumor growth curves. (B) tumorigenic activity assessed by measuring tumor weight. (C) cell metastasis efficiency assessed by measuring lung light radiation intensity. (D) histological inspection was measured by HE staining. (E) METTL3 and EMT markers in lung tissues of mice determined using western blot. All the experiments were repeated at least three times, and data are represented as mean ± SD. These data were analyzed by two-way ANOVA followed by Tukey's post-tests. *$p < 0.05$.

without metastasis within 5 years (n = 21) and patients with metastasis within 5 years (n = 37). METTL3 mRNA expression was found to be significantly higher in metastatic tissues than that in non-metastatic tissues (Fig. 1A). In contrast, the levels of other m6A-related methyltransferases in OS tissues from patients with metastases did not exhibit any prognostic potential (Fig. 1B). Patient survival analysis displayed that the patients with high METTL3 expression suffered from a shorter median survival and a poorer prognostic outcome (Fig. 1C). In addition, METTL3 levels were significantly higher in OS patients at advanced (II-III) Enneking stage (n = 32) than those at lower Enneking stage (I) (n = 26) (Fig. 1D). Further examination of METTL3 protein levels in OS tissue samples using immunohistochemistry revealed that METTL3, significantly localized in the nuclei of OS cells, was strongly positive in metastatic tissues and weakly positive in non-metastatic tissues (Fig. 1E). Consistently, elevated m6A mRNA level was observed in OS patients with metastasis compared with those without metastasis (Fig. 1F).

### 3.2. METTL3 downregulation inhibits cell migration, invasion and EMT process

The expression of METTL3 was detected in OS cells using RT-qPCR, which revealed that METTL3 was significantly elevated in

OS cells and the elevation was more pronounced in Saos2 and HOS cells (Fig. 2A), which had higher metastatic activity. Saos2 and HOS cells were selected as our following *in vitro* subjects. We then transfected sh-METTL3 into Saos2 and HOS cells to verify the effect of METTL3 downregulation on OS cell motility, i.e., cell migration, invasion and EMT. RT-qPCR showed that sh-METTL3 was stably transfected into the Saos2 and HOS cells (Fig. 2B). Wound healing assays showed that diminished METTL3 expression significantly hindered the migratory capacity of Saos2 and HOS cells (Fig. 2C). Correspondingly, Matrigel invasion assay established that the invasion of OS cells was significantly inhibited by METTL3 silencing (Fig. 2D). Next, immunofluorescence was performed to detect whether METTL3 induced the EMT of cells. The reduction of METTL3 simultaneously diminished the expression of the mesenchymal marker Vimentin and conversely augmented the expression of the epithelial marker E-cadherin in OS cells, indicating that the reduction of METTL3 inhibited the EMT in cells (Fig. 2E). It was shown that METTL3 reduction effectively constrained the migration, invasion and EMT of OS cells.

### 3.3. METTL3 downregulation inhibits EMT and metastasis

We next assessed the relevance of METTL3 to OS development and metastasis *in vivo*. The tumor volume and growth rate of Saos2
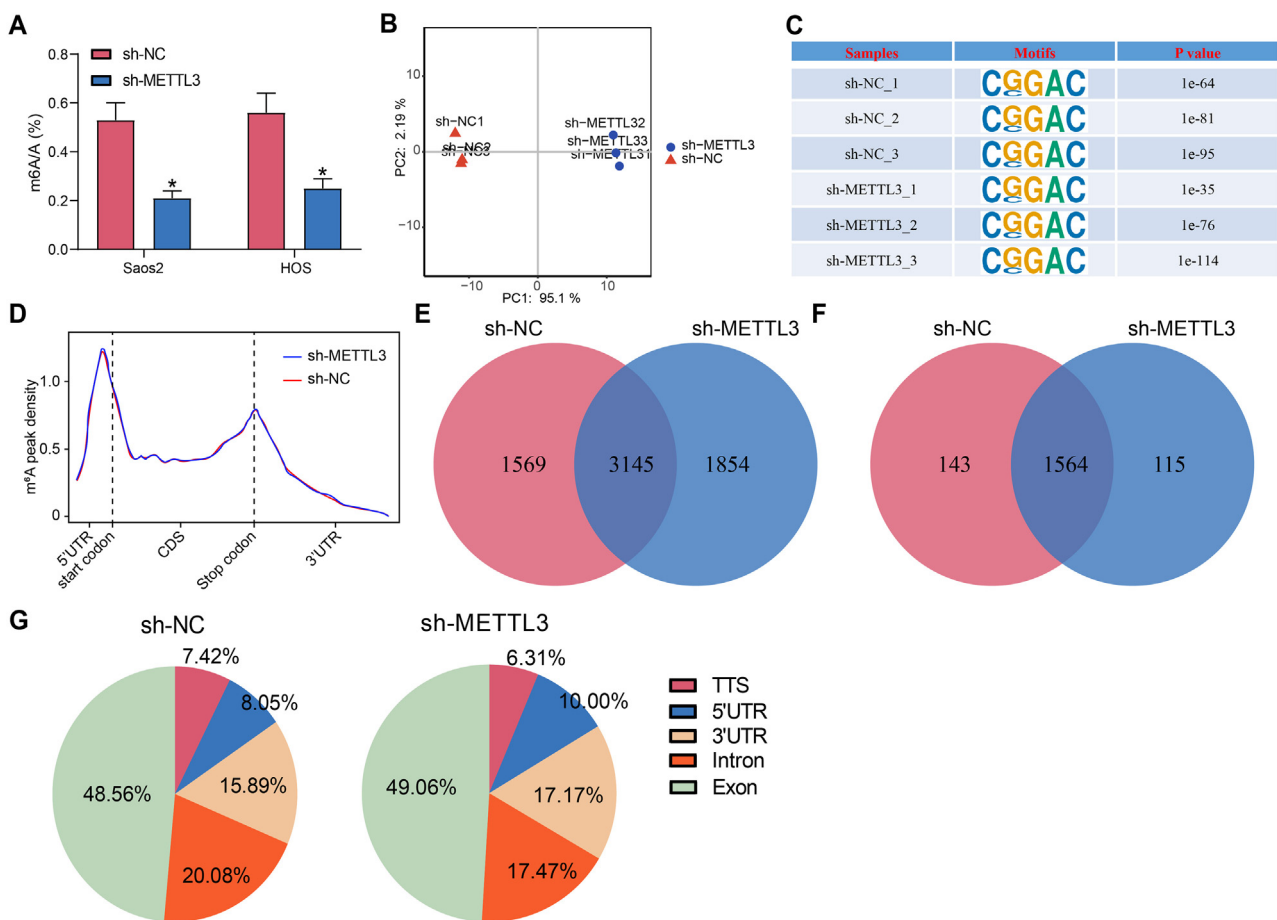


**Fig. 4.** The m6A patterns in OS cells after knockdown of METTL3. (A) m6A analysis of m6A levels in OS cells. (B) experimental reproducibility analyzed by PCA. (C) m6A-seq analysis of GGAC sequences among METTL3 poor expression and control cells. (D) the density distribution of m6A peaks across mRNA transcripts was analyzed by dividing the regions of the 5′UTR, CDS and 3′UTR into 100 fragments, and then determining the percentage of m6A peaks that fell within each fragment. (E) analysis of m6A modification changes in cells after METTL3 knockdown by m6A-seq. (F) analysis of gene modification changes in cells after METTL3 knockdown by m6A-seq. (G) m6A-seq statistics of regions enriched in m6A modifications. All the experiments were repeated at least three times, and data are represented as mean ± SD. These data were analyzed by two-way ANOVA followed by Tukey's post-tests. *$p < 0.05$.
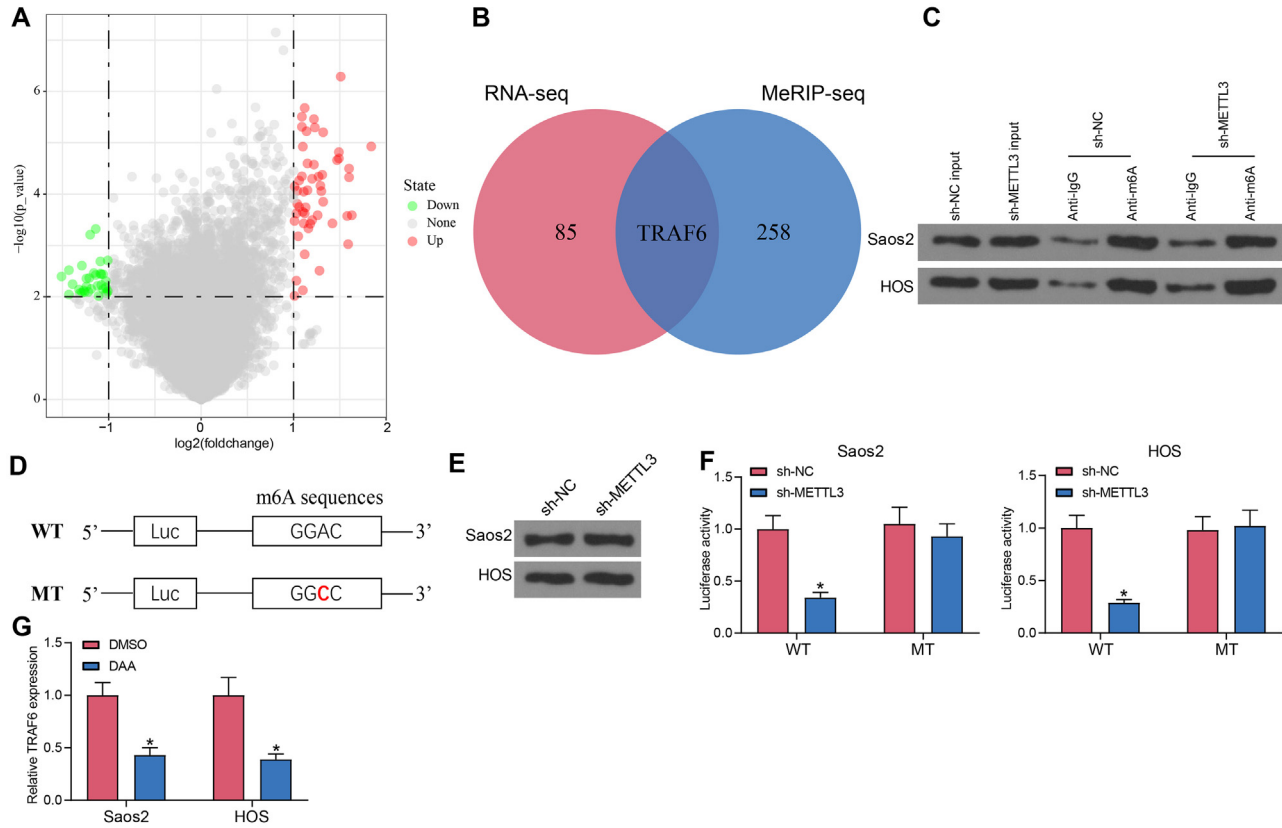
**Fig. 5.** TRAF6 expression is affected by METTL3 in a m6A-dependent manner in OS cells. (A) differentially expressed genes in HOS cells examined using transcriptome sequencing. (B) identification of METTL3 downstream genes by RNA-seq and MeRIP-seq. (C) m6A modifications in OS cells after METTL3 knockdown examined using RIP experiments. (D) construction of MT TRAF6 by modifying the m6A shared sequence. (E) protein expression of MT TRAF6 in METTL3 downregulated cells examined using western blot. (F) the m6A modification of TRAF6 by METTL3 examined using dual-luciferase assay. (G) TRAF6 mRNA expression in cells after DAA treatment using RT-qPCR. All the experiments were repeated at least three times, and data are represented as mean ± SD. These data were analyzed by two-way ANOVA followed by Tukey's post-tests. $^*p < 0.05$.

and HOS cells poorly expressing METTL3 were significantly lower than those of the control group (Fig. 3A). The weight measurement of xenograft tumors removed after 28 days also showed that METTL3 silencing inhibited the development of OS in nude mice (Fig. 3B). Cells were injected into the tail vein, and the location and growth of tumor xenografts were observed in the lungs using luciferase signals. Notably, METTL3 low-expressing cells metastasized less to the lungs, and the intensity of light radiation in the lungs was significantly reduced compared to the control group (Fig. 3C). Histological staining of mouse lungs exhibited a significant decline in the number of nodules in mouse lungs after METTL3 inhibition (Fig. 3D). Also, the result of western blot showed an increase in the epithelial cell marker and a decrease in the mesenchymal cell marker in the metastatic lung nodules of mice harboring METTL3 knockdown (Fig. 3E). In a word, METTL3 plays a fundamental role in promoting OS cell invasion and metastasis.

### 3.4. m6A-regulated genes mediate tumor metastasis

OS cells transfected with sh-METTL3 also showed much lower m6A levels than that in control cells, which also confirmed the role of METTL3 as a writer of m6A (Fig. 4A). To investigate m6A modifications in specific genes, we detected m6A modifications in HOS cells after METTL3 knockdown by m6A-seq. Independent biological replicate experiments followed by principal component analysis (PCA) showed that the three replicate sequences of each sample clustered together, indicating good reproducibility among the three replicate samples of each group (Fig. 4B). The GGAC motif

was highly enriched within the m6A locus in both control and METTL3-downregulated cells (Fig. 4C). The m6A peaks were particularly abundant near the start and stop codons (Fig. 4D). The m6A-seq analysis observed 1569 new m6A peaks and 1854 disappearing m6A peaks in control and METTL3-downregulated cells, respectively, while the remaining 3145 peaks were found in both control and METTL3-downregulated cells (Fig. 4E). For m6A-regulated genes, m6A-seq identified 143 newly modified genes and 115 genes with lost m6A modification in METTL3-downregulated cells, while 1564 other genes were found in both control and METTL3-downregulated cells (Fig. 4F). We further analyzed the total m6A distribution pattern of mRNAs based on the m6A-seq results. Similar patterns of total m6A distribution were found in control and METTL3 downregulated cells, indicating that the m6A peaks were mainly enriched in the exon region. Meanwhile, 5′UTR deposition in cells poorly expressing METTL3 increased from 8.05% to 10.00% and m6A deposition of 3′UTR increased from 15.89% to 17.17% compared to control cells (Fig. 4G). The results suggest that unique peaks and genes in METTL3 downregulated cells are expected to contain real targets.

### 3.5. METTL3 modifies TRAF6 expression via m6A

To investigate the potential targets of METTL3 in OS, we performed transcriptome sequencing to compare the gene expression profiles after METTL3 knockdown in HOS cells. Among them, 29 genes were appreciably downregulated, while 56 genes were drastically upregulated (Fig. 5A). Since METTL3 is a methyltransferase,
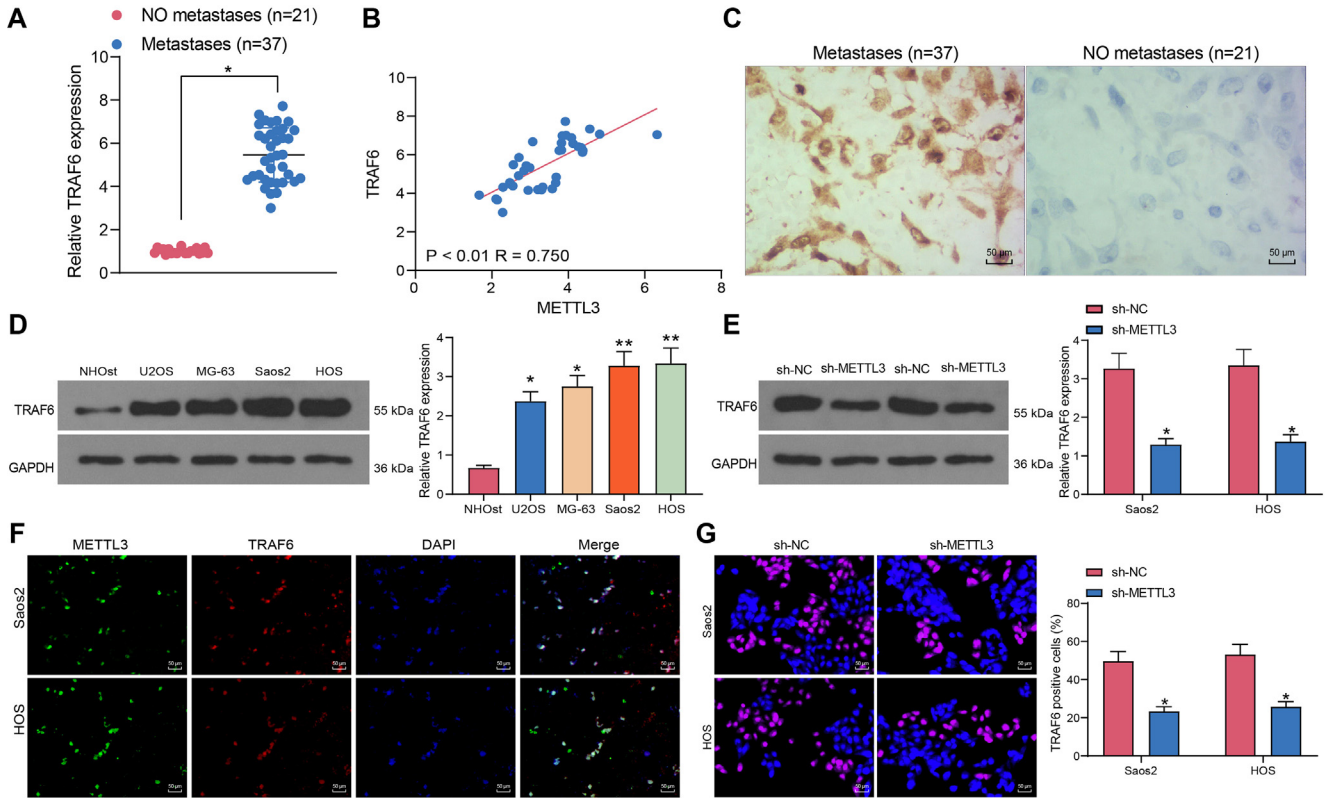
**Fig. 6.** TRAF6 correlates with METTL3 in OS tissues. (A) expression of TRAF6 in OS tissues detected by RT-qPCR. (B) Pearson's correlation analysis of METTL3 and TRAF6 in OS tissues from patients with metastasis. (C) immunohistochemical detection of TRAF6 localization in OS tissues. (D-E) TRAF6 protein expression in OS cells (D) and METTL3 low expressing OS cells (E) determined using western blot. (F) immunofluorescence detection of TRAF6 localization in OS cells. (G) TRAF6-positive cells in METTL3 low expressing cells by immunofluorescence analysis. All the experiments were repeated at least three times, and data are represented as mean ± SD. These data were analyzed by unpaired *t* test, one-way or two-way ANOVA followed by Tukey's post-tests. *$p < 0.05$, **$p < 0.01$.

transcripts carrying hypomethylated m6A peaks after METTL3 knockdown may be the target of METTL3. Filtering for hypomethylated m6A peaks in differentially expressed genes showed that TRAF6 was upregulated in both MeRIP-seq and RNA-seq (Fig. 5B). To further support the idea that METTL3 targets TRAF6 mRNA via m6A modification, western blot was conducted. The results showed that anti-m6A antibody significantly enriched TRAF6 protein levels in OS cells, and additional knocking-down METTL3 significantly decreased the m6A levels of TRAF6 (Fig. 5C). We then constructed luciferase reporter genes containing WT or MT TRAF6 to figure out the impact of m6A modification on TRAF6 expression. For MT TRAF6, the m6A modification was eliminated due to the replacement of adenosine base with cytosine in the m6A shared sequence (RRACH) (Fig. 5D). Knockdown of METTL3 had no significant effect on protein expression of MT TRAF6 (Fig. 5E). The luciferase reporter gene assay showed that the transcript level of WT TRAF6 was significantly reduced in response to sh-METTL3, but MT TRAF6 showed no significant change (Fig. 5F), suggesting that the regulation of TRAF6 levels is controlled by the METTL3-related m6A modification. Notably, inhibition of m6A activity by an inhibitor of RNA methylation DAA greatly reduced TRAF6 mRNA expression (Fig. 5G).

### 3.6. METTL3 is related to TRAF6 expression in OS

To examine the TRAF6 expression modulated by METTL3, RT-qPCR was performed. Detection of TRAF6 expression in OS tissues revealed that TRAF6 was overexpressed in the metastatic OS tis-

sues (Fig. 6A). Moreover, there was a positive correlation between METTL3 and TRAF6 expression in the metastatic OS patients (Fig. 6B). Nuclear localization of TRAF6 in OS tissues was demonstrated by immunohistochemistry, which also showed significantly elevated TRAF6 levels in metastatic OS tissues (Fig. 6C). Western blot showed that TRAF6 protein expression was elevated in OS cells (Fig. 6D) and subsequently decreased in OS cells after knockdown of METTL3 (Fig. 6E). Immunofluorescence staining demonstrated the nuclear localization of TRAF6 (Fig. 6F) and that depletion of METTL3 resulted in loss of TRAF6 expression in OS cells (Fig. 6G). These data suggested that METTL3 positively regulated TRAF6 expression in OS.

### 3.7. TRAF6 reverses the repressive effect of sh-METTL3 on OS cell migration, invasion and EMT

Overexpression vectors of TRAF6 were delivered into METTL3-depleted cells, and western blot exhibited the successful transfection of TRAF6-OE fragment (Fig. 7A). Assessment of TRAF6-mediated cell motility showed that TRAF6 significantly reversed the action of sh-METTL3, resulting in significant increases in cell migration and invasion (Fig. 7B and C). The change of EMT was also detected, and TRAF6 induced Vimentin expression and lowered E-cadherin expression in the OS cells, suggesting EMT was enhanced again in the cells low expressing METTL3 (Fig. 7D). We found that TRAF6 was able to reverse the effects of sh-METTL3, resulting in a significant increase in cell mobility *in vitro*.
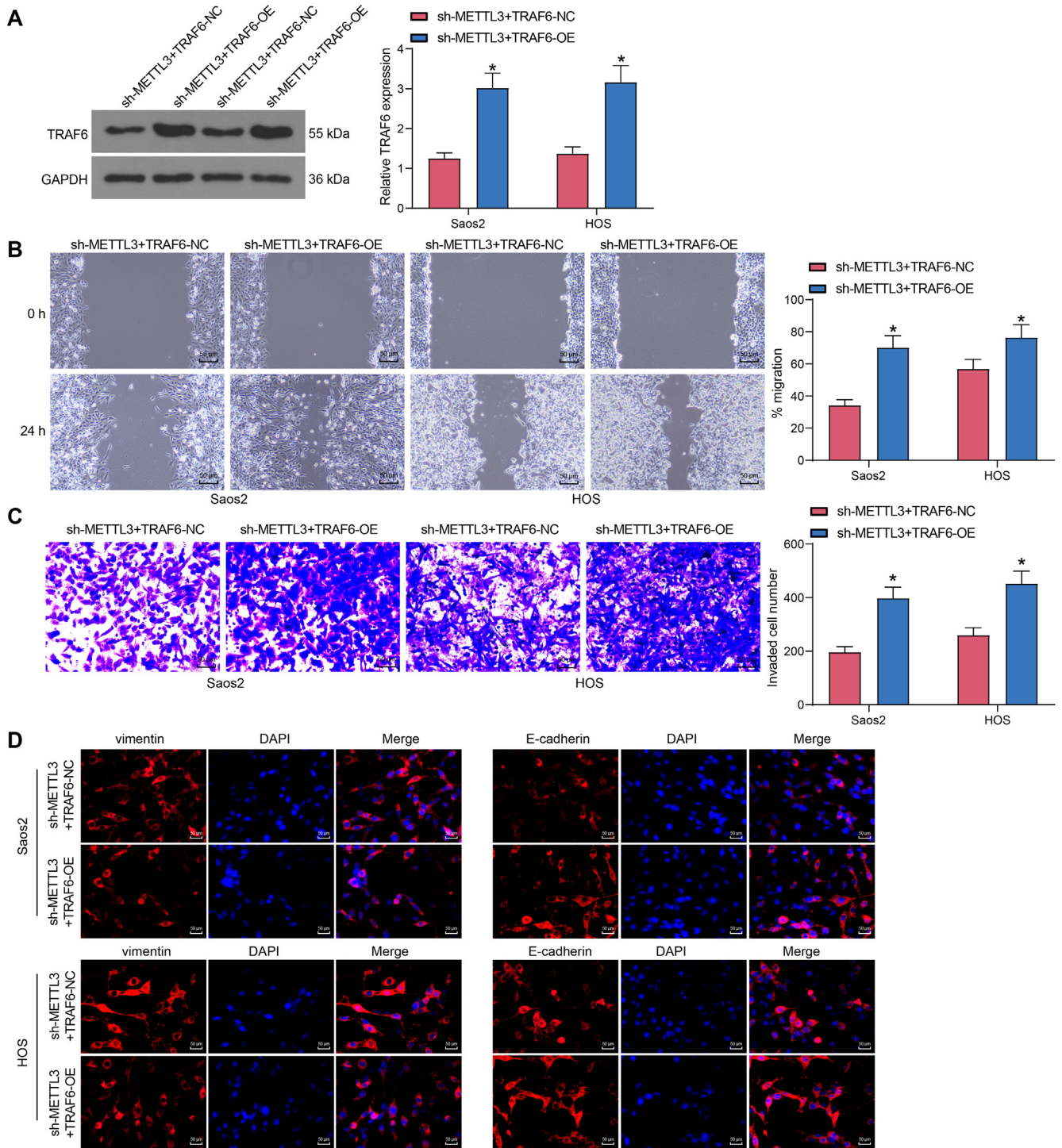
**Fig. 7.** TRAF6 overexpression abrogates the repressive effects of METTL3 silencing on the migration, invasion and EMT of OS cells. OS cells were co-transfected with sh-METTL3 + TRAF6-OE or TRAF6-NC. (A) TRAF6 protein expression in cells determined using western blot. (B) cell migration measured using wound healing assay. (C) invasion of OS cells determined using Matrigel invasion assay. (D) EMT process of OS cells determined using immunofluorescence staining. All the experiments were repeated at least three times, and data are represented as mean ± SD. These data were analyzed by two-way ANOVA followed by Tukey's post-tests. *$p < 0.05$.

### 3.8. TRAF6 reverses the repressive effect of sh-METTL3 on OS metastasis

Tumor volume changes were detected in mice injected with cells after co-transfection. TRAF6 significantly increased the tumor growth rate in mice (Fig. 8A) and elevated the weight of xenograft tumors after 28 days (Fig. 8B). The cells were also injected into tail vein of mice, and the luciferase signal was monitored to visualize

the location and growth of tumor xenografts in the lung. TRAF6 caused a significant augment in the intensity of light radiation in the lung and enhanced the efficiency of metastasis (Fig. 8C). HE staining of mouse lung tissues showed a significant increase in nodules formed in mice induced by TRAF6 (Fig. 8D). Western blot assay of TRAF6 and EMT-related protein expression in lung tissues showed that overexpression of TRAF6 increased EMT in nude mice as well (Fig. 8E). These experiments demonstrated that TRAF6 was
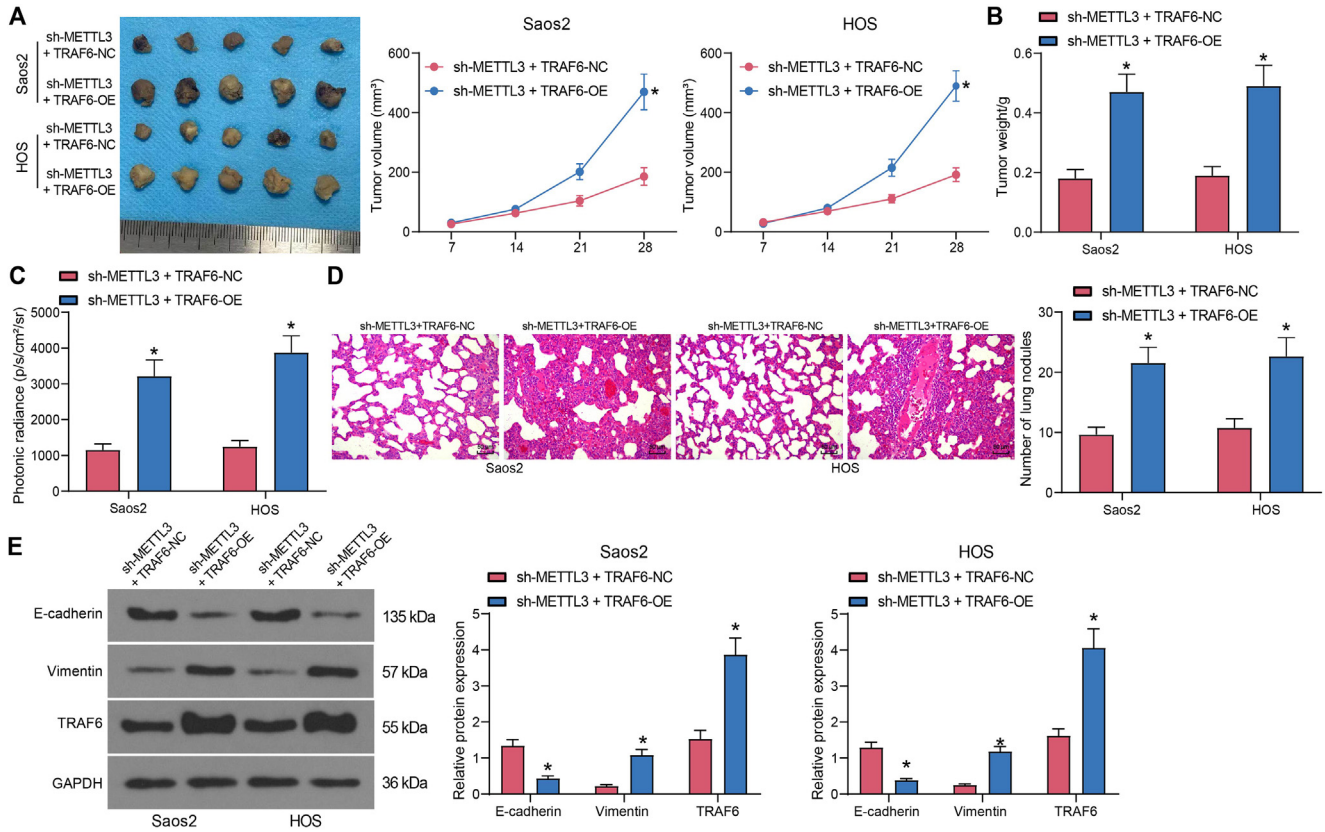
**Fig. 8.** TRAF6 overexpression abrogates the repressive effects of METTL3 silencing on the tumorigenic and metastatic properties of OS cells. (A) tumor images and tumor growth curves. (B) tumorigenic activity assessed by measuring tumor weight. (C) cell metastasis efficiency assessed by measuring lung light radiation intensity. (D) histological inspection was measured by HE staining. (E) TRAF6 and EMT markers in lung tissues of mice determined using western blot. All the experiments were repeated at least three times, and data are represented as mean ± SD. These data were analyzed by two-way ANOVA followed by Tukey's post-tests. $^*p < 0.05$.

able to reverse the effects of sh-METTL3, resulting in a significant elevation in both tumorigenic and metastatic activity of the OS cells.

## 4. Discussion

OS, a bone cancer frequently occurred in children and young adults, is a high-grade cancer characterized by extreme metastases to the lungs [15]. Curative treatment consists of multi-agent chemotherapy and complete surgical resection, and the risk of recurrence is high despite the application of multi-agent chemotherapy [16]. So, the development of new treatment methods for metastatic OS is essential. Evidence has showed that m6A RNA methylation has overwhelming effects on RNA production/metabolism and involves in the pathogenesis of various diseases, including cancers [17,18]. In this study, our results provide fresh insights into the biological role of METTL3 and m6A modification in OS progression. We found significant overexpression of METTL3 in metastatic OS tissues and cell lines. In addition, our data exhibited that the elevated m6A methylated RNA level and expression of METTL3 facilitated OS metastases by promoting TRAF6 expression.

The results of this study displayed that the METTL3 expression in OS tissues from patients with metastases was much higher than that from patients without metastases, which was consistent with a recent study [19]. In addition, the overexpression of METTL3 is highly linked to poor outcomes for patients with OS. Consistently, METTL3 expression was remarkably elevated in gastric cancer tissues, and multivariate Cox regression analysis displayed that

METTL3 expression represents an independent prognostic factor and powerful predictor in patients with gastric cancer [20]. To substantiate the effects of METTL3 *in vitro*, we transfected shRNA targeting METTL3 into Saos2 and HOS cells, which showed higher METTL3 expression among all four OS cell lines. As we expected, depletion of METTL3 impaired the OS cell abilities to migrate and invade, and most importantly, curbed the EMT process, one important step for cancer cell metastasis. In nasopharyngeal carcinoma cells, downregulation of METTL3 inhibited the expression of EMT markers Vimentin and N-cadherin [21]. Deletion of METTL3 has been previously found to downregulate m6A and to inhibit the migration, invasion and EMT of cancer cells via regulating Snail and JUNB, both major transcription factors of EMT [22,23]. Similarly, our *in vivo* experiments showed that OS cells with knockdown of METTL3 formed smaller tumors and had less potential to metastasize to the lung in nude mice. Also, metastatic foci in the liver were observed in orthotopic mice injected with METTL3-overexpressing gastric cancer cells [24]. These results confirmed the tumor-supporting role of METTL3 in OS.

The m6A methyltransferase METTL3 has been reported to promote the progression of various cancers, including bladder cancer and lung cancer, through modulating the expression of microRNAs or mRNAs [25,26]. The similar mechanism was observed in OS as well [27–31]. In this study, through m6A-seq, we revealed that the m6A enrichment region was distributed around the exon, while METTL3 poorly expressing OS cells showed more deposition of m6A in the 5′UTR and 3′UTR. After evaluation of the RNA-seq and MeRIP results, METTL3 was found to epigenetically activate TRAF6 via the m6A-dependent pathway. The binding between

TRAF6 mRNA and METTL3 was corroborated using luciferase reporter and western blot assays. Interestingly, the binding relation between TRAF6 mRNA and METTL3 has been verified in microglia [32]. TRAF6 is a notable oncogene in esophageal squamous cell carcinoma, pancreatic cancer, prostate cancer, nasopharyngeal carcinoma, and gastric cancer [33–37]. Moreover, the expression of Vimentin was downregulated and that of E-cadherin was elevated after TRAF6 knockdown in cancer stem cells of squamous cell carcinoma of head and neck [38], indicating the possible role of TRAF6 in regulating the EMT event. Under the condition of OS, the TRAF6 protein was upregulated in OS tissues from patients with lung metastasis compared to those from patients without lung metastasis [39]. Moreover, small interfering RNA specifically targeting TRAF6 partly reversed the stimulative effects of miR-140-3p inhibitor on EMT, migration, and invasion of U2OS cells [40]. By contrast, pcDNA-TRAF6 reversed the inhibiting effects of miR-146b-5p on cell invasion and migration of OS cells [41], which was large in line with the results of our experiments using both sh-METTL3 and TRAF6-OE.

## 5. Conclusion

Collectively, we expounded the significance of METTL3-dependent m6A modification in OS progression, wherein it supports cancer cell EMT and metastasis. The discovery of the METTL3/TRAF6 axis and its impacts on metastasis might be beneficial for further OS investigation and for developing therapeutic strategies against OS. However, more studies are required to authenticate this hypothesis.

## CRediT authorship contribution statement

**Jing Wang:** Conceptualization, Investigation, Visualization, Data curation, Supervision, Writing – original draft. **Wentao Wang:** Conceptualization, Investigation, Visualization, Data curation, Supervision, Writing – original draft. **Xing Huang:** Conceptualization, Investigation, Visualization, Data curation, Supervision, Writing – original draft. **Jiashi Cao:** Data curation, Formal analysis, Resources, Software, Validation. **Shuming Hou:** Data curation, Formal analysis, Resources, Software, Validation. **Xiangzhi Ni:** Data curation, Formal analysis, Resources, Software, Validation. **Cheng Peng:** Methodology, Project administration, Visualization, Writing – review & editing. **Tielong Liu:** Methodology, Project administration, Visualization, Writing – review & editing.

## Declaration of Competing Interest

The authors declare that they have no known competing financial interests or personal relationships that could have appeared to influence the work reported in this paper.

## Funding

## References

[1] R.A. Durfee, M. Mohammed, H.H. Luu, Review of Osteosarcoma and Current Management, Rheumatol Ther 3 (2) (2016) 221–243.

[2] D.A. Müller, U. Silvan, On the biomechanical properties of osteosarcoma cells and their environment, Int J Dev Biol 63 (1-2) (2019) 1–8.

[3] X. Zhao, Q. Wu, X. Gong, Q. Liu, Y. Ma, Osteosarcoma: a review of current and future therapeutic approaches, Biomed Eng Online 20 (1) (2021) 24.

[4] Q. Lan, P.Y. Liu, J. Haase, J.L. Bell, S. Hüttelmaier, T. Liu, The Critical Role of RNA m(6)A Methylation in Cancer, Cancer Res 79 (7) (2019) 1285–1292.

[5] W. Wei, X. Ji, X. Guo, S. Ji, Regulatory Role of N(6) -methyladenosine (m(6) A) Methylation in RNA Processing and Human Diseases, J Cell Biochem 118 (9) (2017) 2534–2543.

[6] X. Deng, R. Su, X. Feng, M. Wei, J. Chen, Role of N(6)-methyladenosine modification in cancer, Curr Opin Genet Dev 48 (2018) 1–7.

[7] X. Cui, Z. Wang, J. Li, J. Zhu, Z. Ren, D. Zhang, W. Zhao, Y. Fan, D. Zhang, R. Sun, Cross talk between RNA N6-methyladenosine methyltransferase-like 3 and miR-186 regulates hepatoblastoma progression through Wnt/beta-catenin signalling pathway, Cell Prolif 53 (3) (2020) e12768.

[8] L. Liu, X. Liu, Z. Dong, J. Li, Y. Yu, X. Chen, F. Ren, G. Cui, R. Sun, N6-methyladenosine-related Genomic Targets are Altered in Breast Cancer Tissue and Associated with Poor Survival, J Cancer 10 (22) (2019) 5447–5459.

[9] A. Visvanathan, V. Patil, A. Arora, A.S. Hegde, A. Arivazhagan, V. Santosh, K. Somasundaram, Essential role of METTL3-mediated m(6)A modification in glioma stem-like cells maintenance and radioresistance, Oncogene 37 (4) (2018) 522–533.

[10] E. Yankova, W. Blackaby, M. Albertella, J. Rak, E. De Braekeleer, G. Tsagkogeorga, E.S. Pilka, D. Aspris, D. Leggate, A.G. Hendrick, N.A. Webster, B. Andrews, R. Fosbeary, P. Guest, N. Irigoyen, M. Eleftheriou, M. Gozdecka, J.M.L. Dias, A.J. Bannister, B. Vick, I. Jeremias, G.S. Vassiliou, O. Rausch, K. Tzelepis, T. Kouzarides, Small-molecule inhibition of METTL3 as a strategy against myeloid leukaemia, Nature 593 (7860) (2021) 597–601.

[11] M. Chen, L. Wei, C.-T. Law, F.-C. Tsang, J. Shen, C.-H. Cheng, L.-H. Tsang, D.-H. Ho, D.-C. Chiu, J.-F. Lee, C.-L. Wong, I.-L. Ng, C.-M. Wong, RNA N6-methyladenosine methyltransferase-like 3 promotes liver cancer progression through YTHDF2-dependent posttranscriptional silencing of SOCS2, Hepatology 67 (6) (2018) 2254–2270.

[12] J. Li, B. Rao, J. Yang, L. Liu, M. Huang, X. Liu, G. Cui, C. Li, Q. Han, H. Yang, X. Cui, R. Sun, Dysregulated m6A-Related Regulators Are Associated With Tumor Metastasis and Poor Prognosis in Osteosarcoma, Front Oncol 10 (2020) 769.

[13] Q. Meng, W. Zhang, X. Xu, J. Li, H. Mu, X. Liu, L. Qin, X. Zhu, M. Zheng, The effects of TRAF6 on proliferation, apoptosis and invasion in osteosarcoma are regulated by miR-124, Int J Mol Med 41 (5) (2018) 2968–2976.

[14] H. Liu, S. Tamashiro, S. Baritaki, M. Penichet, Y. Yu, H. Chen, J. Berenson, B. Bonavida, TRAF6 activation in multiple myeloma: a potential therapeutic target, Clin Lymphoma Myeloma Leuk 12 (3) (2012) 155–163.

[15] F. Jafari, J. Javdansirat, S. Sanaie, A. Naseri, A. Shamekh, D. Rostamzadeh, S. Dolati, Osteosarcoma: A comprehensive review of management and treatment strategies, Ann Diagn Pathol 49 (2020) 151654, https://doi.org/10.1016/j.anndiagpath.2020.151654.

[16] A. Smrke, Y.B. Tam, P.M. Anderson, R.L. Jones, P.H. Huang, The perplexing role of immuno-oncology drugs in osteosarcoma, J Bone Oncol 31 (2021) 100400.

[17] X.Y. Chen, J. Zhang, J.S. Zhu, The role of m(6)A RNA methylation in human cancer, Mol Cancer 18 (1) (2019) 103.

[18] S. Garbo, C. Zwergel, C. Battistelli, m6A RNA methylation and beyond – The epigenetic machinery and potential treatment options, Drug Discov Today 26 (11) (2021) 2559–2574.

[19] W. Zhang, L. Wang, P. Zhang, Q. Zhang, m6A regulators are associated with osteosarcoma metastasis and have prognostic significance: A study based on public databases, Medicine (Baltimore) 100 (20) (2021) e25952.

[20] Q. Wang, C. Chen, Q. Ding, Y. Zhao, Z. Wang, J. Chen, Z. Jiang, Y. Zhang, G. Xu, J. Zhang, J. Zhou, B. Sun, X. Zou, S. Wang, METTL3-mediated m(6)A modification of HDGF mRNA promotes gastric cancer progression and has prognostic significance, Gut 69 (7) (2020) 1193–1205.

[21] Z.F. Liu, J. Yang, S.P. Wei, X.G. Luo, Q.S. Jiang, T. Chen, Y.Q. Gong, Upregulated METTL3 in nasopharyngeal carcinoma enhances the motility of cancer cells, Kaohsiung J Med Sci 36 (11) (2020) 895–903.

[22] X. Lin, G. Chai, Y. Wu, J. Li, F. Chen, J. Liu, G. Luo, J. Tauler, J. Du, S. Lin, C. He, H. Wang, RNA m(6)A methylation regulates the epithelial mesenchymal transition of cancer cells and translation of Snail, Nat Commun 10 (1) (2019) 2065.

[23] S. Wanna-udom, M. Terashima, H. Lyu, A. Ishimura, T. Takino, M. Sakari, T. Tsukahara, T. Suzuki, The m6A methyltransferase METTL3 contributes to Transforming Growth Factor-beta-induced epithelial-mesenchymal transition of lung cancer cells through the regulation of JUNB, Biochem Biophys Res Commun 524 (1) (2020) 150–155.

[24] B. Yue, C. Song, L. Yang, R. Cui, X. Cheng, Z. Zhang, G. Zhao, METTL3-mediated N6-methyladenosine modification is critical for epithelial-mesenchymal transition and metastasis of gastric cancer, Mol Cancer 18 (1) (2019) 142.

[25] J. Han, J.Z. Wang, X. Yang, H. Yu, R. Zhou, H.C. Lu, W.B. Yuan, J.Z. Lu, Z.J. Zhou, Q. Lu, J.F. Wei, H. Yang, METTL3 promote tumor proliferation of bladder cancer by accelerating pri-miR221/222 maturation in m6A-dependent manner, Mol Cancer 18 (1) (2019) 110.

[26] D. Jin, J. Guo, Y. Wu, J. Du, L. Yang, X. Wang, W. Di, B. Hu, J. An, L. Kong, L. Pan, G. Su, m(6)A mRNA methylation initiated by METTL3 directly promotes YAP translation and increases YAP activity by regulating the MALAT1-miR-1914-3p-YAP axis to induce NSCLC drug resistance and metastasis, J Hematol Oncol 12 (1) (2019) 135.

[27] Z. Ling, L. Chen, J. Zhao, m6A-dependent up-regulation of DRG1 by METTL3 and ELAVL1 promotes growth, migration, and colony formation in osteosarcoma, Biosci Rep 40 (4) (2020).

[28] H. Liu, G. Qin, Y. Ji, X. Wang, H. Bao, X. Guan, A. Wei, Z. Cai, Potential role of m6A RNA methylation regulators in osteosarcoma and its clinical prognostic value, J Orthop Surg Res 16 (1) (2021) 294.

[29] W. Miao, J. Chen, L. Jia, J. Ma, D. Song, The m6A methyltransferase METTL3 promotes osteosarcoma progression by regulating the m6A level of LEF1, Biochem Biophys Res Commun 516 (3) (2019) 719–725.

[30] C. Zhou, Z. Zhang, X. Zhu, G. Qian, Y. Zhou, Y. Sun, W. Yu, J. Wang, H. Lu, F. Lin, Z. Shen, S. Zheng, N6-Methyladenosine modification of the TRIM7 positively regulates tumorigenesis and chemoresistance in osteosarcoma through ubiquitination of BRMS1, EBioMedicine 59 (2020) 102955.

[31] L. Zhou, C. Yang, N. Zhang, X. Zhang, T. Zhao, J. Yu, Silencing METTL3 inhibits the proliferation and invasion of osteosarcoma by regulating ATAD2, Biomed Pharmacother 125 (2020) 109964.

[32] L. Wen, W. Sun, D. Xia, Y. Wang, J. Li, S. Yang, The m6A methyltransferase METTL3 promotes LPS-induced microglia inflammation through TRAF6/NF-kappaB pathway, Neuroreport (2020).

[33] K. Aripaka, S.K. Gudey, G. Zang, A. Schmidt, S.S. Åhrling, L. Österman, A. Bergh, J. von Hofsten, M. Landström, TRAF6 function as a novel co-regulator of Wnt3a target genes in prostate cancer, EBioMedicine 45 (2019) 192–207.

[34] L. Kong, X. Li, H. Wang, G. He, A. Tang, Calycosin inhibits nasopharyngeal carcinoma cells by influencing EWSAT1 expression to regulate the TRAF6-related pathways, Biomed Pharmacother 106 (2018) 342–348.

[35] Y. Rong, D. Wang, W. Wu, D. Jin, T. Kuang, X. Ni, L. Zhang, W. Lou, TRAF6 is over-expressed in pancreatic cancer and promotes the tumorigenicity of pancreatic cancer cells, Med Oncol 31 (11) (2014) 260.

[36] M. Yang, M. Jin, K. Li, H. Liu, X. Yang, X. Zhang, B. Zhang, A. Gong, Q. Bie, TRAF6 Promotes Gastric Cancer Cell Self-Renewal, Proliferation, and Migration, Stem Cells Int 2020 (2020) 3296192.

[37] F. Yao, Q. Han, C. Zhong, H. Zhao, TRAF6 promoted the tumorigenicity of esophageal squamous cell carcinoma, Tumour Biol 34 (5) (2013) 3201–3207.

[38] L. Chen, Y.C. Li, L. Wu, G.T. Yu, W.F. Zhang, C.F. Huang, Z.J. Sun, TRAF6 regulates tumour metastasis through EMT and CSC phenotypes in head and neck squamous cell carcinoma, J Cell Mol Med 22 (2) (2018) 1337–1349.

[39] Q. Meng, M. Zheng, H. Liu, C. Song, W. Zhang, J. Yan, L. Qin, X. Liu, TRAF6 regulates proliferation, apoptosis, and invasion of osteosarcoma cell, Mol Cell Biochem 371 (1-2) (2012) 177–186.

[40] Q. Guo, N. Zhang, S. Liu, Z. Pang, Z. Chen, By targeting TRAF6, miR-140-3p inhibits TGF-beta1-induced human osteosarcoma epithelial-to-mesenchymal transition, migration, and invasion, Biotechnol Lett 42 (11) (2020) 2123–2133.

[41] M. Jiang, W. Lu, X. Ding, X. Liu, Z. Guo, X. Wu, p16INK4a inhibits the proliferation of osteosarcoma cells through regulating the miR-146b-5p/TRAF6 pathway, Biosci Rep 39 (2) (2019).